Structural and optoelectronic properties of sprayed Sb:SnO_2 thin films: Effects of substrate temperature and nozzle-to-substrate distance

A. R. Babar, S. S. Shinde, A. V. Moholkar, C. H. Bhosale, and K. Y. Rajpure†

Electrochemical Materials Laboratory, Department of Physics, Shivaji University, Kolhapur-416004, India

Abstract: The influence of substrate temperature and nozzle-to-substrate distance (NSD) on the structural, morphological, optical and electrical properties of Sb:SnO_2 thin films prepared by chemical spray pyrolysis has been analyzed. The structural, morphological, optical and electrical properties were characterized by using XRD, SEM, UV-visible spectrophotometry and Hall effect measurement techniques. It was seen that the films are polycrystalline, having a tetragonal crystal structure with strong orientation along the (200) reflection. The pyramidal crystallites formed due to coalescence were observed from SEM images. The values of highest conductivity, optical transmittance and figure of merit of about 1449 $(\Omega\cdot\text{cm})^{-1}$, 70 % and 5.2×10^{-3} $\square/\Omega$, respectively, were observed for a typical film deposited using optimal conditions (substrate temperature = 500 ℃ and NSD = 30 cm).

Key words: substrate temperature; NSD; structural; optoelectronic properties

DOI: 10.1088/1674-4926/32/10/102001 **EEACC:** 2520

1. Introduction

Transparent conducting oxides (TCOs), like SnO_2, In_2O_3 and ZnO, have a wide range of applications in optoelectronic devices, owing to their unique combination of high electrical conductivity and optical transparency in the visible spectrum of light[1−3]. The development of TCO coatings seems to be an important application of thin film technology, which works as window layers transparent to solar radiation and electrical contacts. Among the TCOs, antimony-doped tin oxide (ATO), being an n-type, wide band gap semiconductor ($\geqslant$ 3.6 eV) with special properties (high transmittance in the visible range and high reflectance in the infrared, excellent electrical conductivity, greater carrier mobility and good mechanical stability), is used in different devices, like solar cells as transparent, protective electrodes, flat panel collectors as spectral selective windows, sensors for the detection of gases, sodium lamps and varistors[4−7].

ATO films have been prepared by various techniques, such as chemical vapour deposition, metalorganic deposition, RF sputtering, electron beam evaporation, sol–gel, pulsed laser deposition and spray pyrolysis[8−12]. Spray pyrolysis is one of the simplest deposition techniques employed in various kinds of thin films due to its simplicity, and its compatibility with large area coatings without high vacuum ambience. Furthermore, the capital cost and the production cost of high quality metal oxide thin films is lowest for sprayed thin films. Moreover, the spray pyrolysis technique is well suited to controlling the texture via the tuning deposition temperature and mass production capability for uniform large area coatings.

Vasu *et al.*[13] have observed that the nozzle-to-substrate distance (NSD) is significant in the pyrolytic reaction, whether it is homogeneous or heterogeneous. It is known that the homogeneous reaction (which affects, the conductivity and the visible transparency of the SnO_2, films) can be minimized by adjusting the substrate temperature and NSD. Shanthi *et al.*[14] reported that the substrate temperature, NSD and air flow rate play a significant role in determining the size distribution of the droplets in the pyrolytic reaction. By suitably adjusting these parameters, it is possible to force a heterogeneous reaction to take place in the vapour phase. Ni *et al.*[15] have reported the electrical, structural, photoluminescence and optical properties of p-type conducting antimony-doped SnO_2 thin films deposited on the quartz glass. By employing a simplified version of spray technique using a perfume atomizer, the synthesis of antimony doped tin oxide (ATO) films is reported by Ravichandran *et al.*[16]. Thangaraju *et al.*[17] have carried out structural and electrical studies on highly conducting spray deposited fluorine and antimony doped SnO_2 thin films from a $SnCl_2$ precursor and reported the lowest sheet resistance (R_{sh}) of 5.65 $\Omega/\square$ with 70% transmittance.

Even though an enormous amount of literature is available on the synthesis and characterization of ATO thin films by different methods, efforts are still going on to enhance their properties–especially the figure of merit, which requires high conductivity and optical transmittance. This study focuses on structural, morphological, optical and electrical properties of sprayed ATO thin films, prepared specially, in order to enhance the conductivity, carrier concentration, electron mobility and figure of merit by varying the substrate temperature and NSD.

2. Experimental methods

Antimony doped tin oxide thin films were prepared by spray pyrolysis onto the glass substrates using AR grade stannic chloride ($SnCl_4\cdot5H_2O$) and antimony trichloride ($SbCl_3$) as precursors. Firstly, the 2M stannic chloride solution in aqueous media was prepared followed by 2 at% antimony incorporation in order to achieve an appropriate doping concentration. For each deposition, 10 cc from this solution was mixed with 10 cc of propane-2-ol to make a final spraying solution of 20 cc. To enhance the physicochemical properties of deposited films,

† Corresponding author. Email: rajpure@yahoo.com
Received 6 March 2011, revised manuscript received 14 June 2011

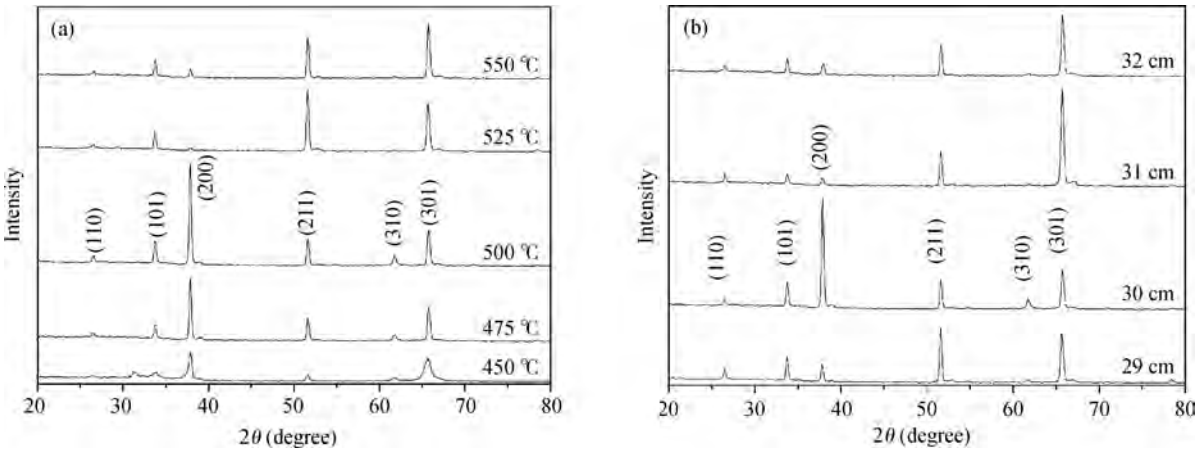

Fig. 1. (a) XRD patterns of Sb:SnO_2 thin films deposited at 450, 475, 500, 525 and 550 ℃. (b) XRD patterns of Sb:SnO_2 thin films deposited with different nozzle-to-substrate distance (NSDs) of 29, 30, 31 and 32 cm.

Table 1. Various parameters estimated for sprayed Sb:SnO_2 thin films with substrate temperature. R_{sh}-Sheet resistance, ρ-Resistivity, n-Carrier concentration, μ-Mobility, ϕ-Figure of merit, E_f-Fermi energy, l-Mean free path, C.S.-Crystallite size, ω_p-plasma frequency, λ_p-plasma wavelength.

Substrate temperature (℃)	R_{sh} (Ω)	ρ (10^{-4} Ω·cm)	n (10^{20} cm^{-3})	μ ($cm^2/(V\cdot s)$)	ϕ (10^{-3} Ω^{-1})	E_f (eV)	l (Å)	C.S. (nm)	ω_p (10^{15} Hz)	λ_p (nm)
450	10.31	12.9	2.46	19.63	0.029	0.53	25.1	19.6	1.91	986
475	8.25	10.6	2.81	20.85	0.175	0.58	27.8	29.9	2.04	923
500	4.21	6.9	3.73	24.04	5.81	0.70	35.2	30.6	2.35	801
525	5.75	8.1	3.36	22.88	2.00	0.65	23.4	28.3	2.23	844
550	7.15	9.7	3.26	19.81	0.602	0.64	27.8	28	2.20	857

we have studied the effect of substrate temperature and NSD from 450 to 550 ℃ and 29 to 32 cm, respectively. After deposition, all the films were allowed to cool naturally to room temperature. The other deposition parameters were kept at their constant values.

The structural properties were studied by a powder X-ray diffractometer (Bruker D8 Advance, France) using CuKα radiation in the 2θ range of 20°–80°. The surface morphology of the films was studied using scanning electron microscopy (SEM, JEOL JSM 6360, Japan). An optical absorption study was carried out in the wavelength range 300–1100 nm using a double beam spectrophotometer (SHIMADZU UV-1700, Japan). The Hall effect setup (supplied by Scientific Equipments, Roorkee, India) was used for the measurement of electrical parameters like carrier concentration (n) and mobility (μ) at room temperature. The electrical conductivity was measured in a van der Pauw configuration. A specially designed Hall probe on a printed circuit board was used to fix the sample of the size 10×10 mm^2. Silver paste was employed to ensure good electrical contacts.

3. Results and discussion

3.1. X-ray diffraction

Figure 1(a) shows the XRD patterns of Sb:SnO_2 thin films as a function of substrate temperature. It shows the polycrystalline nature with a preferred orientation along the (200) reflection. The comparison of observed and standard d values confirms that SnO_2 has a tetragonal crystal structure[18]. As the temperature increases, the reflection intensity of the planes increases up to 500 ℃, while for higher temperature the reorientation effect is observed. From this it is seen that the substrate temperature has a key role in the growth mechanism. Deposited films shows strong intense reflection along the (200) plane up to 500 ℃, and further at 525 and 550 ℃ the (211) and (301) observe highly intense orientations, respectively. The films deposited at 450–500 ℃ show preferred orientation along the (200) plane[19]. Other weak intensity peaks viz. (110), (101) and (310) are also observed.

In order to study the effect of NSD on the structural properties, SnO_2 films were grown by varying the NSD from 29 to 32 cm, at a fixed substrate temperature of 500 ℃. The XRD patterns of Sb:SnO_2 thin films deposited at different NSDs are shown in Fig. 1(b). It is observed that the film deposited with a 29 cm NSD shows orientation along the (211) plane, whereas for higher NSDs (30 cm, 31cm, 32 cm) the films show orientations along the (200) and (301) crystallographic directions. The higher intensity of the (200) reflection is observed for the films deposited at a 30 cm NSD. The orientation along the (301) plane at higher NSDs is due to a reorientation effect caused due to heterogeneous reactions responsible for the film structure. From the above structural analysis it is indicated that the (211) and (301) reflections become dominant with changing nozzle-to-substrate distance

The crystallite size 'D' is calculated using Scherrer's formula,

$$D = \frac{0.9\lambda}{\beta \cos\theta}, \quad (1)$$

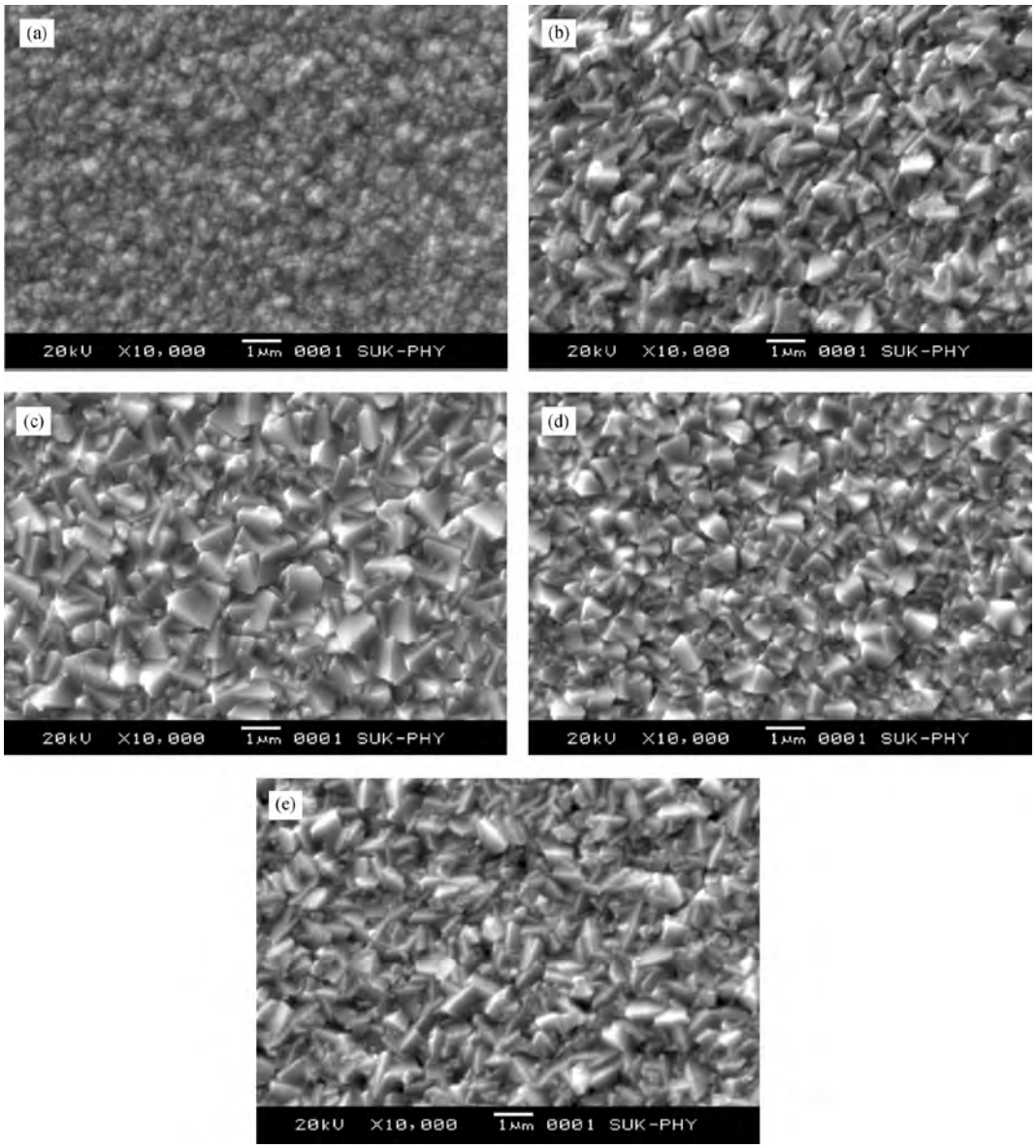

Fig. 2. Scanning electron micrographs of Sb:SnO_2 thin films deposited at (a) 450 ℃, (b) 475 ℃, (c) 500 ℃, (d) 525 ℃ and (e) 550 ℃.

where D is the crystallite size, β is the broadening of the diffraction line measured at half of its maximum intensity (rad) FWHM and λ is the X-ray wavelength (1.5406 Å). It is seen (Table 1) that as the temperature increases, the average crystallite size increases up to 500 ℃ (19.6 to 30.6 nm) and tends to decrease afterwards due to a homogeneous reaction occurring above the surface of the substrates.

3.2. Scanning electron microscopy

Figures 2(a)–2(e) show the SEM images of Sb:SnO_2 thin films deposited at different substrate temperatures. It is seen that the films are rough, homogenous, compact and adherent in nature. The film thickness and grain size of the films increases with deposition temperature from 450 to 550 ℃. The presence of big and faceting nanocrystals observed in these figures indicates the fact that pyramidal crystallites are formed by coalescence. At 450 ℃, randomly oriented spherical grains are observed. At higher temperatures, these spherical grains are converted into needle, prismatic, pyramidal like grains. In the present study, two principal factors, such as substrate temperature and condensation rate, determine the structure of the condensate. SnO_2 in the tetragonal phase belongs to the P42/mnm space group and has a ditetragonal–dipyramidal type of symmetry. This means that the external shape of the macrocrystals is a combination of prisms (lateral facets of the crystal) and pyramids (end facets of the crystal). It is observed that long prismatic and needle crystals are formed at higher crystallization rates in comparison with rates of pyramidal formation. At intermediate rates, there is a combination of these cases, with comparable areas of prismatic and pyramidal facets. Cross-sectional images (Fig. 3) show the thickness variation of the deposited films. As the temperature increases, the thickness of the film goes on increasing (1.25–1.64 μm) up to 500 ℃ and then decreases for higher temperatures.

Figure 4 shows scanning electron micrographs of the Sb:SnO_2 samples deposited for various NSDs. The film deposited at 29 cm shows a relatively rough, loosely bound and

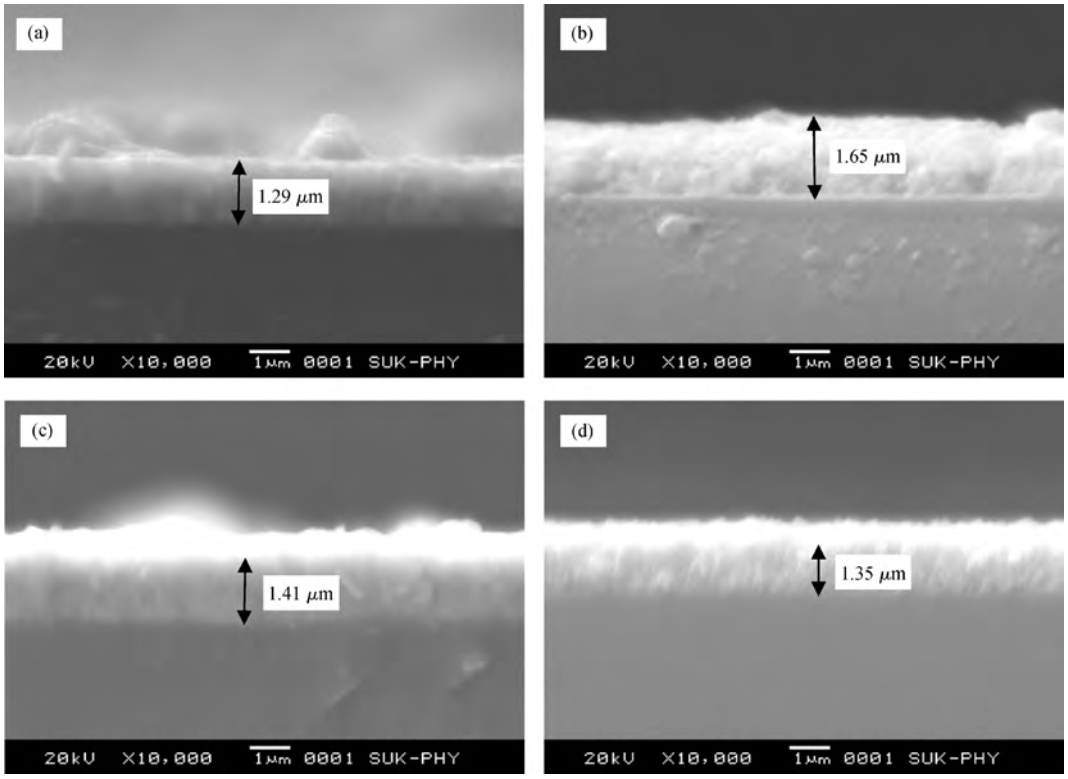

Fig. 3. Cross-sectional images of Sb:SnO_2 thin films deposited at (a) 475 ℃, (b) 500 ℃, (c) 525 ℃ and (d) 550 ℃.

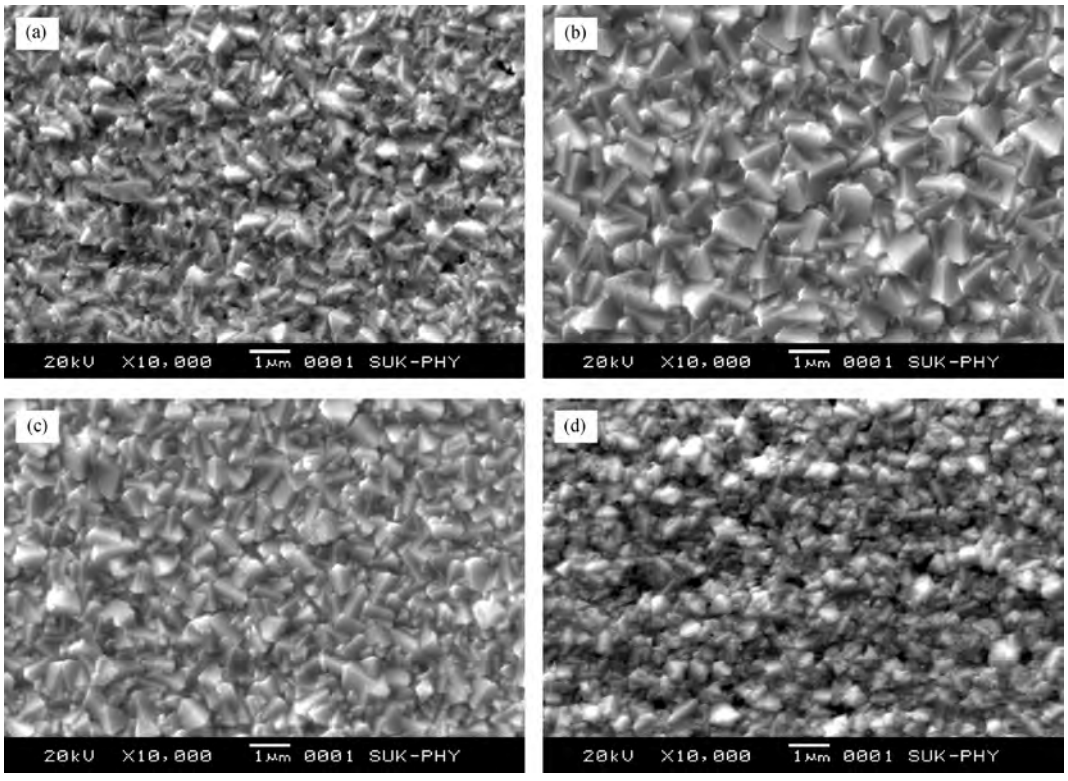

Fig. 4. Scanning electron micrographs of Sb:SnO_2 thin films deposited with different NSDs of (a) 29 cm, (b) 30 cm, (c) 31 cm and (d) 32 cm.

slightly porous surface morphology while the film deposited at a 30 cm NSD shows uniformly distributed grains of greater size. After 30 cm, films were transferred towards loosely organized smaller grains. Cross-sectional images of different NSDs are shown in Fig. 5. The thickness of the films goes on decreasing (1.7–1.29 μm) with increasing NSD due to the evaporation of aerosols. The nature of the film structure changing with thickness can be considered as evidence of layer-by-layer growth during spray pyrolysis. This means that when a certain thickness is achieved, crystallites stop growing and new

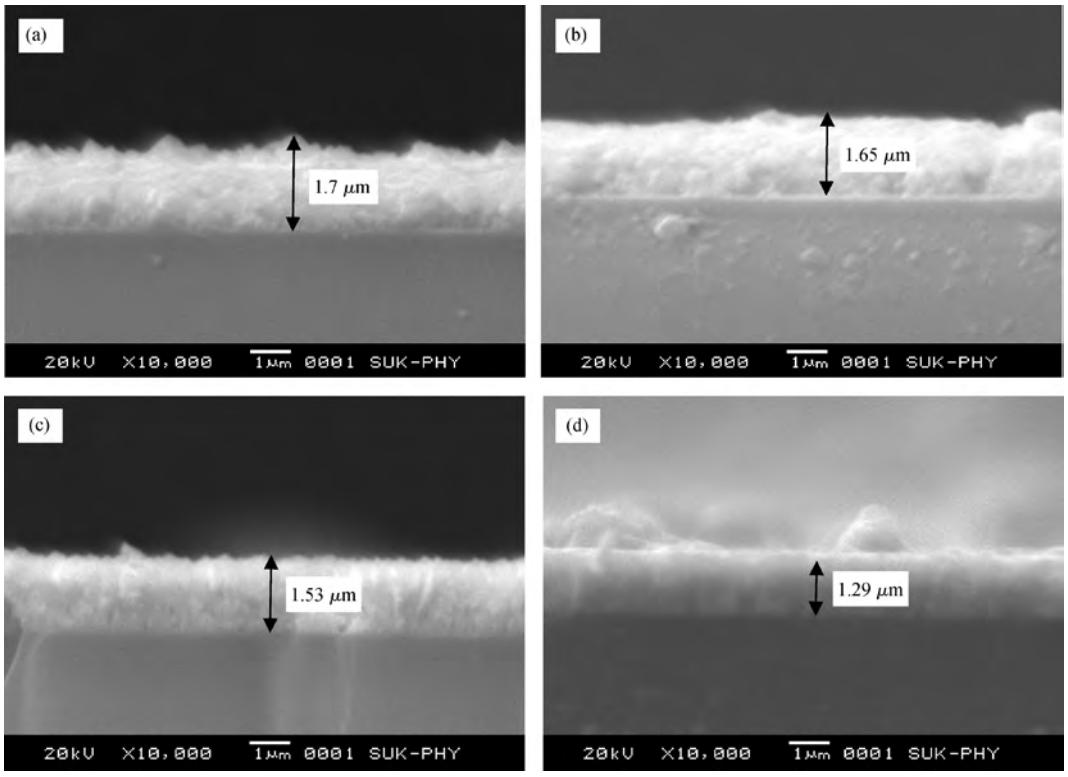

Fig. 5. Cross-sectional images of Sb:SnO_2 thin films deposited with different NSDs of (a) 29 cm, (b) 30 cm, (c) 31 cm and (d) 32 cm.

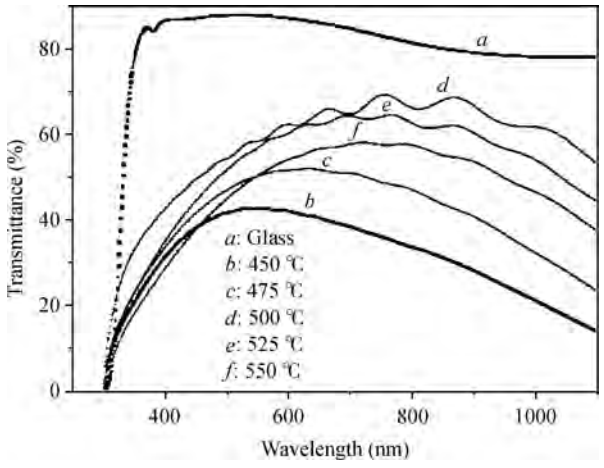

Fig. 6. Optical transmittance of Sb:SnO_2 films at different substrate temperatures using a NSD of 30 cm.

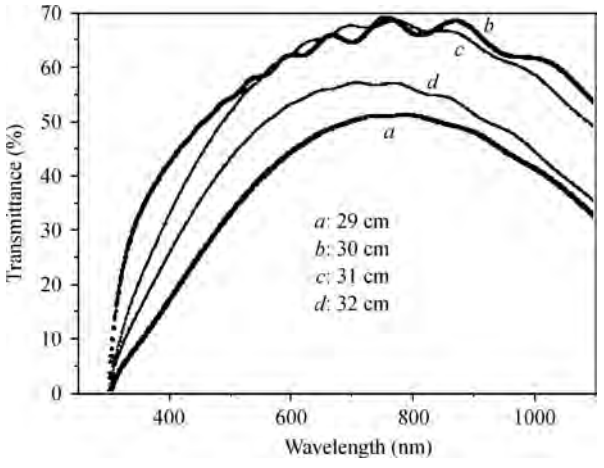

Fig. 7. Optical transmittance of Sb:SnO_2 films deposited with different NSDs.

crystallites are appearing on the surface. In other words, deposited films may have layering structure where every layer would have its own structure with other sizes of crystallite and their preferred orientation.

3.3. Optical properties

Figures 6 & 7 show the variation in optical transmittance with wavelength of SnO_2:Sb thin films deposited at various substrate temperatures and NSDs. The well-developed interference patterns in transmittance (T) show that the films are specular to a great extent. The average transmission in the visible region has been found to be 70% at the optimized substrate temperature of 500 ℃. At lower temperatures, e.g. at 450 ℃, relatively lower transmission is observed due to the formation of whitish milky films due to incomplete decomposition of the sprayed droplets. The increase in optical transmission with substrate temperature can be attributed to the increase in structural homogeneity and crystallinity. In general, in the visible region of the spectrum, the transmission is very high (high enough to observe interference fringes). Owing to less absorption due to transfer of electrons from the valence band to the conduction band as a result of optical interference effects, it is possible to maximize the transmission of the thin film at a particular region of wavelengths. The decrease in transmittance at higher temperature (> 500 ℃) may be due to the increased scattering

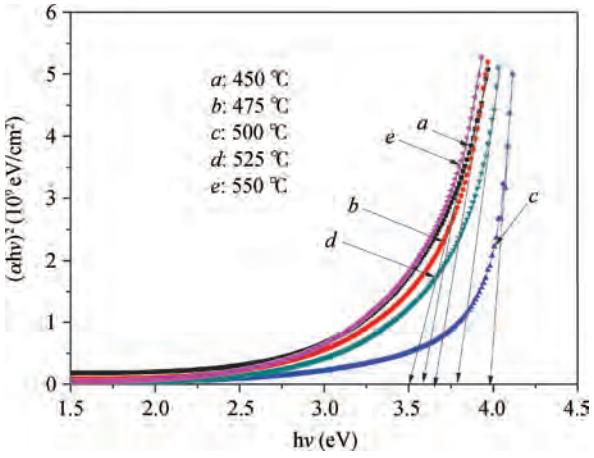

Fig. 8. Plot of $(\alpha h\nu)^2$ versus $h\nu$ for Sb:SnO_2 thin films deposited with different substrate temperatures.

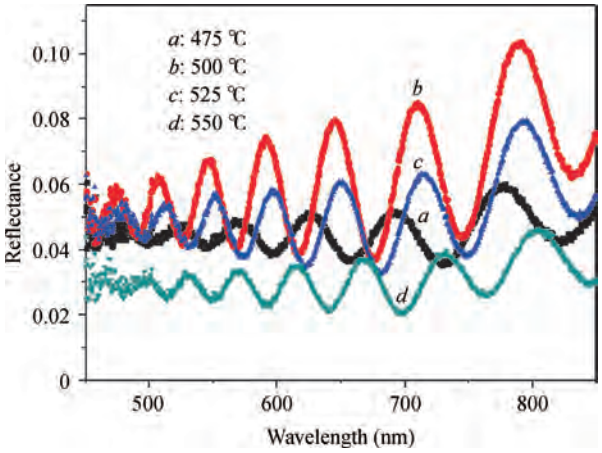

Fig. 10. Variation in reflectance of Sb:SnO_2 thin films with various substrate temperatures.

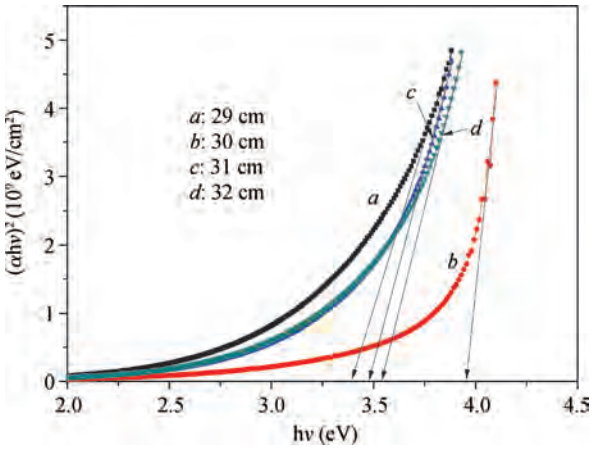

Fig. 9. Plot of $(\alpha h\nu)^2$ versus $h\nu$ for Sb:SnO_2 thin films deposited with different NSDs.

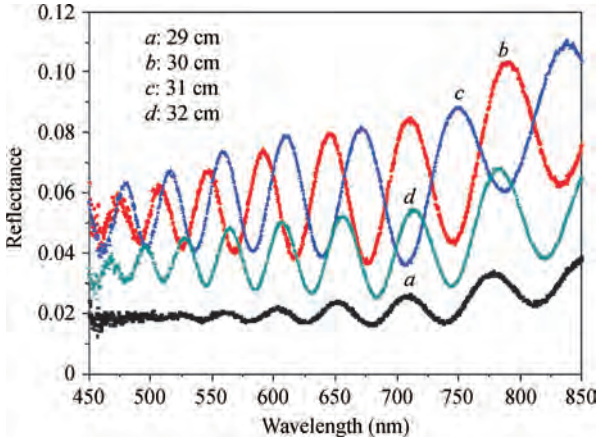

Fig. 11. Variation in reflectance of Sb:SnO_2 thin films prepared with different NSDs.

of photons by crystal defects. The free carrier absorption of photons may also contribute to the reduction in optical transmittance[20]. The amplitude of interference fringes decreased at higher temperatures (> 500 ℃), and this indicated a loss in surface smoothness leading to slight scattering losses.

The variation in transmission of the deposited films with NSD is shown in Fig. 7. The transmittance increases with NSDs from 50% to 70%, achieving maximum value at 30 cm. Lower transmittance at lower NSDs is because of sprayed solution droplets reaching the substrate early, so the mechanism of spray pyrolysis will not be completed perfectly. Also, the resulting films are rough and whitish-blue in colour, which may be one of the reasons for a lower transmittance. At the optimum NSD, the thermal energy gained by the droplet is such that it vaporizes just above the substrate and gives a good, highly transparent film. In the case of a high NSD, the droplets vaporize entirely above the nucleation centre of the film onto the preheated substrates. Hence the homogeneous reaction takes place in the vapour phase, which diminishes the deposition efficiency and the molecules condense as microcrystallites. They form a powdery precipitate on the substrate, resulting in a decrease in transparency. The decrease in optical transmittance at higher NSDs is due to re-crystallization of the crystallites in the film.

In order to estimate the band gap energy of the films, the variation in $(\alpha h\nu)^2$ with $h\nu$ is shown in Figs. 8 and 9 for various substrate temperatures and NSDs. This has a straight line portion, indicating that the transition involved is direct allowed[21]. The direct band gap, determined by extrapolating the straight portion to the energy axis to $(\alpha h\nu)^2 = 0$, varies from 3.50 to 3.97 eV up to 500 ℃ (30 cm NSD) and further decreases for higher temperatures and NSDs. These values are higher than the value of $E_g = 3.57$ eV reported for single crystal SnO_2[22]. This increase in band gap can be attributed to an increase in carrier concentration of the films due to complete decomposition of the deposited materials. Thin films often show a small band gap widening and the absorption edge moves to a shorter wavelength than that of the bulk material showing blue shift. So the blue shift of the band gap is attributed to the compressive strain in deposited tin oxide films, and after increasing the deposition temperature and NSD, the band-gap value decreases due to the relaxation of the built in strain.

Reflectance spectra of Sb:SnO_2 thin films deposited with various substrate temperatures and NSDs are shown in Figs. 10 and 11. The reflectance increases with increasing substrate temperature and NSD, attaining a maximum value at 500 ℃

Table 2. Various parameters estimated for sprayed Sb:SnO_2 thin films with various NSDs. R_{sh}-Sheet resistance, ρ-Resistivity, n-Carrier concentration, μ-Mobility, ϕ-Figure of merit, E_f-Fermi energy, l-Mean free path, C.S.-Crystallite size, ω_p-Plasma frequency, λ_p-Plasma wavelength.

Nozzle to substrate distance (cm)	R_{sh} (Ω)	ρ (10^{-3} Ω·cm)	n (10^{20} cm^{-3})	μ (cm^2/(V·s))	ϕ (10^{-3} Ω^{-1})	E_f (eV)	l (Å)	C.S. (nm)	ω_p (10^{15} Hz)	λ_p (nm)
29	7.36	1.2	2.79	17.87	0.17	0.57	23.8	25.7	2.03	926
30	4.21	69	3.73	24.04	5.81	0.70	35.2	30.6	2.35	801
31	6.57	0.1	3.35	18.48	2.68	0.65	26.1	29.6	2.23	845
32	8.53	1.1	3.18	17.79	0.57	0.63	24.7	25.6	2.17	867

and 30 cm NSD and decreasing afterwards. Well resolved interference patterns are seen. The reflectivity of the films increases with respect to wavelength. The IR reflectivity of the films is calculated using the relation[23]

$$R = (1 + 2\varepsilon_0 c_0 R_{sh})^{-2}, \quad (2)$$

where free space impedance $1/\varepsilon_0 c_0 = 376\ \Omega$, R_{sh} is sheet resistance. This equation is valid over a wide range of IR region. The calculated IR reflectivity is found to be in the range of 89%–96% and 91%–96% for the films prepared with various substrate temperatures and NSDs. The estimated high IR reflectance of these films suggests that the films are useful in flat plate collectors and in different electrode processes.

Drude's model is generally used for the analysis of a decrease in the transmittance near the infrared region[24]. Briefly, this model illustrates the drop in transmittance at the near IR region and it is associated with the plasma frequency (ω_p) expressed as

$$\omega_p = \left(\frac{4\pi n e^2}{\varepsilon_0 \varepsilon_\infty m_c^*}\right)^{1/2}, \quad (3)$$

where n is the carrier concentration, e is the electronic charge, ε_0 is the permittivity of free space, ε_∞ is the high-frequency permittivity and m_c^* is the effective mass. As ω_p is proportional to the square root of the carrier concentration, an increase in carrier concentration leads to a decrease in transmission in the near-IR region. The plasma wavelength (λ_p) is expressed as

$$\lambda_p^2 = \frac{4\pi^2 c^2}{\omega_p^2}. \quad (4)$$

As the deposition temperature and NSD increase, the plasma wavelength shifts towards the lower wavelength side due to increases in carrier concentration (Table 2) and then shifts towards the higher wavelength region due to a decrease in carrier concentration at higher substrate temperature as well as NSDs.

The device performance is determined from the figure of merit (ϕ) and is calculated by using Hacke's formula,

$$\phi = \frac{T^{10}}{R_{sh}}, \quad (5)$$

where T is the transmittance and R_{sh} is the sheet resistance. The sheet resistance (R_{sh}) is a main factor for figure of merit, which is calculated by the van der Pauw technique. The variation in figure of merit with substrate temperature and NSD is shown in Tables 1 and 2. The highest achieved figure of merit is about 5.02×10^{-3} Ω^{-1} at 500 ℃ and 30 cm NSD and it is attributed to enhanced crystallinity.

3.4. Electrical properties

The electrical resistivity (ρ) and Hall mobility (μ) of the Sb:SnO_2 thin films with different deposition temperature are shown in Table 1. The resistivity is found to decrease with increasing temperature initially up to 500 ℃ and then increases for higher temperatures. The initial decrease in resistivity with temperature up to 500 ℃ is a consequence of an increase in mobility, which is found to increase due to the improvement of the crystalline structure of the films due to heating, as observed by the XRD analysis. With increased crystallinity, grain size increases thereby minimizing the grain boundary scattering losses and defects in the films. So the number of electron trap states decreases and hence the carrier concentration increases. Further, the resistivity increases above 500 ℃ temperatures due to evaporation of solution and slight generation of powdery films. The Hall mobility and carrier concentration of films represents a similar trend as per resistivity. The electron motilities and carrier concentration for Sb:SnO_2 films range from 19 to 25 cm^2/(V·s) and 2.46×10^{20} to 3.73×10^{20} cm^{-3}, respectively. On the other hand, it is generally agreed that the stoichiometry of the films is commanded by the deposition atmosphere and substrate temperature. In case of films deposited at low substrate temperatures, the overall of Sn oxide reactions do not take place. As the substrate temperature increases, films with a more appropriate stoichiometry are obtained. For films deposited at higher substrate temperatures, the following two aspects should be considered: a more stoichiometric film is formed, and a diffusion of alkaline impurities coming from the substrate to the films is present; both facts lead to Sb:SnO_2 films being more resistive.

Table 2 shows the variation in electrical properties of the Sb:SnO_2 films grown at different NSDs. As the NSD changes, the thermal gradient in the vapour space changes, hence modification in the thermophoretic force acting on the liquid droplet takes place. The expression for the thermophoretic force (F_{th}) is[25]

$$F_{th} = \frac{-3\pi\eta r \,\mathrm{grad} T_d}{\gamma_a \lambda_a}, \quad r \ll l, \quad (6)$$

$$\mathrm{grad} T_d = \frac{3\lambda_a \mathrm{grad} T_a}{2\lambda_a + \lambda_d}, \quad (7)$$

where r is the radius of the droplet, T_d is the temperature of the droplet, T_a is the temperature of air, λ_a is the thermal conductivity of air, λ_d is the thermal conductivity of the droplet, η is the viscosity, γ_a is the density, and l is the mean free path of air molecules. In spray pyrolysis, when the droplet approaches the substrate, it should vaporize entirely just above

the substrate; this is the ideal condition for the best transportation of the species to the substrate. The thermal energy gained by the droplet depends on the factor grad T_d. Assuming that the size distribution of all the droplets is the same, the thermal energy gained by the droplets will increase greatly with increasing NSD. This results in the preheating of the droplets by carrier gas through heat radiation. It is known that preheating enhances the pyrolytic reaction[14]. As the NSD increases, the grain growth increases, which turn decreases scattering. The structural quality of the films increases with the NSD and hence a reduction in the grain-boundary scattering is obtained in addition to the grain size growth. Therefore, it seems that at 30 cm NSD, a heterogeneous reaction takes place due to the preheating of the optimized droplet size and hence good Sb:SnO_2 quality films are obtained. Above 30 cm, the thermal energy gained by the droplet is very high, causing the complete vaporization of water molecules (oxidizing agent in the pyrolytic decomposition) takes place far away from the substrate. The particle melts and vaporizes (or sublimes), and a chemical reactions occur in the vapour phase. This is a homogeneous reaction, because all the reactant molecules and product molecules are in the vapour phase. The molecules condense as microcrystallites, which form a powdery precipitate on the substrate. This powder disturbs the formation of the layer and leads to a reduction in transmission. In addition, the homogeneous reaction diminishes the deposition efficiency. The variation in mobility with NSD can be explained on the basis of grain boundary scattering and impurity scattering, which are the main scattering phenomena in the case of extrinsic semiconductors.

The mean free path (l) is calculated by the following relation,

$$l = \frac{h}{2e}\left(\frac{3n}{\pi}\right)^{1/3}\mu, \tag{8}$$

where h is Plank's constant, e is the electron charge, n is the carrier concentration and μ is the Hall mobility. The mean free path increases with deposition temperature and NSD (Tables 1 & 2), and then decreases for higher deposition temperature and NSD. The films deposited at 500 ℃ and 30 cm NSD show a mean free path (l) of 35.2 Å. Since the l values are considerably shorter than the grain size (as seen in the SEM images), the Hall mobility is limited by the ionized impurity scattering rather than the grain boundary scattering.

The film degeneracy is confirmed by evaluating the Fermi energy using relation

$$\Delta E = \frac{h^2}{8m^*}\left(\frac{3n}{\pi}\right)^{2/3}. \tag{9}$$

The value of effective mass evaluated from plasma frequency for Sb:SnO_2 films; $0.27m_e$ (m_e = rest mass of electron) is used for the evaluation of Fermi energy. The calculated value of Fermi energy lies in the range of 0.53–0.70 eV (Table 2). Fermi energy values are relatively higher compared to kT at room temperature, which is evidence for the degenerate nature of materials.

4. Conclusions

The influence of the substrate temperature (T_s) and NSD on the structural, morphological, optical and electrical properties of Sb:SnO_2 thin films has been investigated. Deposited films show a tetragonal crystal structure with a reorientation effect. Morphological images show that the surface of the films is rough and adherent. Thermophoretic forces affect the nucleation growth of the films. The blue shift has been observed in optical band gap analysis. The highest achieved transparency and conductivity at the optimized substrate temperature and NSD is about 70% and 1449 $(\Omega\cdot\text{cm})^{-1}$, respectively. With these properties, the deposited Sb:SnO_2 films are very useful in optoelectronic devices.

Acknowledgement

One of the authors (A.R. Babar) is very grateful to the University Grants Commission, New Delhi, for financial support through a UGC meritorious fellowship.

References

[1] Ginley D S, Bright C. Transparent conducting oxides. MRS Bulletin, 2000, 25: 15

[2] Hartnagel H L, Dawar A L, Jain A K, et al. Semiconducting transparent thin films. Bristol: Institute of Physics Publishing, 1995

[3] Minami T. Transparent conducting oxide semiconductors for transparent electrodes. Semicond Sci Technol, 2005, 20: 35

[4] Kanai N, Nuda T, Ueta K, et al. Photocatalytic efficiency of TiO_2/SnO_2 thin film stacks prepared by DC magnetron sputtering. Vacuum, 2004, 74: 723

[5] Peng S, Cheng F, Liang J, et al. Facile solution-controlled growth of $CuInS_2$ thin films on FTO and TiO_2/FTO glass substrates for photovoltaic application. J Alloys Compd, 2009, 481: 786

[6] Dima A, Dima O, Moldovan C, et al. Substrate influence on the response of sol–gel derived SnO_2 gas-sensors. Thin Solid Films, 2003, 427: 427

[7] Lee D S, Kim Y T, Huh J S, et al. Fabrication and characteristics of SnO_2 gas sensor array for volatile organic compounds recognition. Thin Solid Films, 2002, 416: 271

[8] Zhang D, Tao L, Deng Z, et al. Surface morphologies and properties of pure and antimony-doped tin oxide films derived by sol–gel dip-coating processing. Mater Chem Phys, 2006, 100: 275

[9] Jung D W, Park D W. Synthesis of nano-sized antimony-doped tin oxide (ATO) particles using a DC arc plasma jet. Appl Surf Sci, 2009, 255: 5409

[10] Li Y Q, Wang J L, Fu S Y, et al. Facile synthesis of antimony-doped tin oxide nanoparticles by a polymer-pyrolysis method. Mater Res Bull, 2010, 45: 677

[11] Jain G, Kumar R. Electrical and optical properties of tin oxide and antimony doped tin oxide films. Opt Mater, 2004, 26: 27

[12] Montero J, Herrero J, Guillén C. Preparation of reactively sputtered Sb-doped SnO_2 thin films: structural, electrical and optical properties. Solar Energy Mater Solar Cells, 2010, 94: 612

[13] Vasu V, Subrahmanyam A. Electrical and optical properties of pyrolytically sprayed SnO_2 film dependence on substrate temperature and substrate-nozzle distance. Thin Solid Films, 1990, 189: 217

[14] Shanthi S, Subramanian C, Ramasamy P. Preparation and properties of sprayed undoped and fluorine doped tin oxide films. Mater Sci Eng B, 1999, 57: 127

[15] Ni J, Zhao X, Zheng X, et al. Electrical, structural, photoluminescence and optical properties of p-type conducting, antimony-doped SnO_2 thin films. Acta Mater, 2009, 57: 278

[16] Ravichandran K, Philominathan P. Fabrication of antimony doped tin oxide (ATO) films by an inexpensive, simplified spray technique using perfume atomizer. Mater Lett, 2008, 62: 2980
[17] Thangaraju B. Structural and electrical studies on highly conducting spray deposited fluorine and antimony doped SnO_2 thin films from $SnCl_2$ precursor. Thin Solid Films, 2002, 402: 71
[18] Joint Committee on Powder Diffraction Standards (JCPDS) Data Card No. 46-1088
[19] Rozati S M. The effect of substrate temperature on the structure of tin oxide thin films obtained by spray pyrolysis method. Mater Character, 2006, 57: 150
[20] Kumar P M R, Kartha C S, Vijayakumar K P, et al. On the properties of indium doped ZnO thin films. Semicond Sci Technol, 2005, 20: 120
[21] Yadav A A, Masumdar E U, Moholkar A V, et al. Effect of quantity of spraying solution on the properties of spray deposited fluorine doped tin oxide thin films. Physica B, 2009, 404: 1874
[22] Summit R M, Borrelli J A. The ultraviolet absorption edge of stannic oxide (SnO_2). J Phys Chem Solids, 1964, 25: 1465
[23] Frank G, Kauer E, Kostlin H. Transparent heat-reflecting coatings based on highly doped semiconductors. Thin Solid Films, 1981, 77: 107
[24] Marcel C, Naghavi N, Couturier G, et al. Scattering mechanisms and electronic behavior in transparent conducting $Zn_xIn_2O_{x+3}$ indium-zinc oxide thin films. J Appl Phys, 2002, 91: 4291
[25] Siefert W. Corona spray pyrolysis: a new coating technique with an extremely enhanced deposition efficiency. Thin Solid Films, 1984, 120: 267